

1 Differentiating between crop and soil effects on soil moisture 2 dynamics

3 Helen Scholz¹, Gunnar Lischeid^{2,3}, Lars Ribbe¹, Ixchel Hernandez Ochoa⁴, Kathrin Grahmann²

4 ¹Institute for Technology and Resources Management in the Tropics and Subtropics (ITT), TH Köln, Cologne, Germany

5 ²Leibniz Centre for Agricultural Landscape Research (ZALF), Müncheberg, Germany

6 ³Institute for Environmental Sciences and Geography, University of Potsdam, Potsdam, Germany

7 ⁴Institute of Crop Science and Resource Conservation (INRES), Crop Science Group, University of Bonn, Bonn, Germany

8 *Correspondence to:* kathrin.grahmann@zalf.de

9 **Abstract.** There is urgent need for developing sustainable agricultural land use schemes. On the one side, climate change is
10 expected to increase drought risk as well as the frequency of extreme precipitation events in many regions. On the other side,
11 crop production has induced increased greenhouse gas emissions and enhanced nutrient and pesticide leaching to groundwater
12 and receiving streams. Consequently, sustainable management schemes require sound knowledge of site-specific soil
13 hydrological processes, accounting explicitly for the interplay between soil heterogeneities and crops. In this study, we apply
14 a principal component analysis to a set of 64 soil moisture time series from a diversified cropping field featuring seven distinct
15 crops and two weeding management strategies.

16 About 97% of the spatial and temporal variance of the data set was explained by the first five principal components.
17 Meteorological drivers accounted for 72.3% of the variance, 17.0% was attributed to different seasonal behaviour of different
18 crops. While the third (4.1%) and fourth (2.2%) principal component explained effects of soil texture and cropping schemes
19 on soil moisture variance, respectively, the effect of soil depth was represented by the fifth component (1.7%). However,
20 neither topography nor weed control had a significant effect on soil moisture variance. Contrary to common expectations, soil
21 and rooting pattern heterogeneity seemed not to play a major role. Findings of this study highly depend on local conditions.
22 However, we consider the presented approach generally applicable to a large range of site conditions.

23 1 Introduction

24 Agriculture plays a major role to ensure the provision of food to a growing global population. At the same time, climate change
25 is putting yield stability at risk due to extreme weather events, rising the need for sustainable management of resources, such
26 as water and soil (Trnka et al., 2014). As part of the adaptation to more challenging conditions, the transformation from large
27 homogeneously cropped fields towards diversified agricultural landscape was identified not only to have positive effects on
28 multiple ecosystem services (Tamburini et al., 2020), but also on the system's resilience to climatic extremes (BIRTHAL and
29 Hazrana, 2019). Additionally, crop diversification is highly beneficial by reducing soil erosion through permanent soil cover
30 (Paroda et al., 2015), and by improving resource use efficiency through wider crop rotations (Rodriguez et al., 2021). In terms
31 of soil water dynamics, crop and management diversification can lead to improved water-stable macro-aggregation, reduced

32 soil compaction and increased soil organic carbon from which soil water infiltration and retention can be positively affected
33 (Alhameid et al., 2020; Fischer et al., 2014; Karlen et al., 2006; Koudahe et al., 2022; Nunes et al., 2018).

34 However, as the diversity of independent variables in agricultural systems increases, demands for frequency and spacing of
35 soil moisture measurements and related data interpretation grow. Therefore, soil sensing networks are receiving increased
36 attention, particularly in Precision Agriculture (PA) (Bogena et al., 2022; Salam and Raza, 2020), where the main goal is to
37 increase efficiency and productivity at the farm level, while minimizing the negative impacts on the environment (Taylor and
38 Whelan, 2010). Soil sensor networks can meaningfully contribute to PA as they can be used for various purposes, including
39 the delineation of management zones (Khan et al., 2020; Salam and Raza, 2020). Still, one of the most important demands to
40 be fulfilled by soil sensing networks is soil moisture monitoring, as accurate measurement of soil water content can play an
41 important role in improving water management and therefore, crop yields (Salam, 2020).

42 Wireless solutions, for instance based on LoRaWAN (Long Range Wide Area Network) technology, in combination with
43 electromagnetic soil moisture sensors avoid labour-intensive and destructive soil moisture measurements that disrupt field
44 traffic. The development of such wireless soil monitoring networks enables broad and affordable application also in areas with
45 low cellular coverage (Cardell-Oliver et al., 2019; Lloret et al., 2021; Placidi et al., 2021; Prakosa et al., 2021).

46 The evolvement of such systems does not only have benefits for management but is also of high relevance for fostering the
47 understanding of hydrological dynamics in the vadose zone. High-resolution datasets measured under real farming conditions
48 can be used to characterize and analyse spatio-temporal dynamics of soil water. Due to the large size of data sets that are
49 recorded with wireless sensor networks, sophisticated data analysis approaches are required to detect hidden patterns and
50 determine influence factors on soil moisture variability (Vereecken et al., 2014). Methods include geostatistical analysis
51 (Vereecken et al., 2014) or data driven approaches (Hong et al., 2016). With the introduction of multiple-points geostatistics,
52 it became possible to not only analyse patterns but also connect them with factors affecting soil moisture, such as topography,
53 texture, crop growth and water uptake, and land management (Brocca et al., 2010; Strebelle et al., 2003). Wavelet analysis can
54 analyse both localized features as well as spatial trends through which non-stationary variation of soil properties can be
55 considered (Si, 2008). Cross-correlation analysis allowed linking soil moisture variability to climatic variables (Mahmood et
56 al., 2012). Furthermore, temporal stability analyses detect spots in the investigated area which are consistently wetter or drier
57 than the mean soil moisture (Baroni et al., 2013; Vachaud et al., 1985, Vanderlinden et al., 2012). This method was already
58 successfully used to detect soil moisture patterns related to soil properties, vegetation, and topography (Zhao et al., 2010).

59 Principal component analysis (PCA) is another method that was successfully applied for soil moisture variability analysis at
60 the field (Hohenbrink et al., 2016; Hohenbrink and Lischeid, 2015; Martini et al., 2017), catchment (Korres et al., 2010;
61 Lischeid et al., 2017; Nied et al., 2013), and regional (Joshi and Mohanty, 2010) scale. These studies build on previous
62 applications in climatology where the term “Empirical Orthogonal Functions” is used (Bretherton et al., 1992). Space and time
63 dimensions can be disentangled and be assigned to influencing factors. Additionally, the propagation of hydrological signals
64 (e.g. precipitation events) over depth can be assessed (Hohenbrink et al., 2016). This opens up great opportunities for
65 contributing to the knowledge of changing soil-hydrological dynamics in complex diversified agricultural systems with

66 increasing heterogeneity and site-specific adjustment of crops, soil types and field management which, to our knowledge, have
67 hardly been studied so far.

68 We analysed a high-resolution soil moisture data set measured by a novel underground LoRaWAN monitoring system with
69 TDR sensors in different depths of the vadose zone at a spatial-temporally diversified agricultural field in Northeast Germany.
70 The novelty of this Internet of underground Things (IouT) soil moisture monitoring network is characterized by its unique on-
71 farm installation environment and the deployment of 180 sensors in up to 0.9 m soil depth, allowing high spatio-temporal
72 resolution wireless data transmission, and enabling conventional farming practices like machinery traffic, tillage and
73 mechanical weeding. The main objective of this study was to identify the drivers of soil moisture variability in a diversified
74 cropping field in terms of crop selection, soil type and field management by applying PCA. Special focus was put on the
75 interpretation of spatial and temporal effects of crop diversification and of soil heterogeneities on soil moisture dynamics.

76 **2 Materials and methods**

77 **2.1 Study site**

78 The study site (52°26'51.8"N 14°08'37.7"E, 66-83 m.a.s.l.) is located near the city of Müncheberg in the federal state of
79 Brandenburg in Northeastern Germany. The landscape is classified as a hummocky ground moraine that formed during the
80 last glacial periods. Glacial and interglacial processes as well as subsequent erosion resulted in highly heterogeneous soils
81 (Deumlich et al., 2018), being classified as Dystric Podzoluvisols according to the FAO scheme (Fischer et al., 2008). In the
82 top 0.3 m soil layer, total organic carbon was 0.94% and total nitrogen content was 0.07%, and pH was 6.12. Between January
83 1991 and December 2020, the mean annual temperature in Müncheberg was 9.6°C, and the mean annual sum of precipitation
84 was 509 mm (DWD Climate Data Center (CDC), 2021).

85 **2.2 Experimental setup**

86 The data collection was carried out from December 2020 until mid of August 2021 in the patchCROP experiment (Grahmann
87 et al, 2021; Donat et al., 2022). This landscape experiment has been set up to study the multiple effects of cropping system
88 diversification on productivity, crop health, soil quality, and biodiversity. To that end, a cluster analysis was carried out based
89 on soil maps and multi-year (2010 to 2019) yield data to identify high and low yield potential zones in the 70-ha large field
90 (Donat et al., 2022). Afterwards, single experimental units comprising 30 patches with an individual size of 0.52 ha (72 m ×
91 72 m) each, have been implemented in both, high and low yield potential zones where each of those zones is characterized by
92 varying soil conditions and a site-specific five-year, legume-based crop rotation (Grahmann et al., 2021). The remaining area
93 outside of the 30 patches was planted with winter rye. For the current study, twelve out of 30 patches were considered (Table
94 1). In the cropping season 2020/2021, seven different main crops were grown. For subsequent data interpretation, crops have
95 been grouped into A) winter crops, B) fallow, followed by summer crops and C) cover crops, followed by summer crops. In
96 seven out of twelve considered patches, weed control was carried out with herbicide application, referred as “conventional”

97 pesticide application, while in the remaining five patches, “reduced” pesticide management was carried out by mainly using
98 mechanical weeding, by harrowing, blind harrowing, and hoeing. Only in the case of high weed pressure herbicides were
99 applied. Due to the potential impact of mechanical weeding, i.e., on rainwater infiltration, soil evaporation and topsoil rooting
100 intensity, we differentiate between these modes of weed control.

101 **2.3 Data collection**

102 Soil moisture was recorded by a long-range-wide-area network (LoRaWAN) based monitoring system. In each patch, one
103 Dribox box equipped with a SDI-12 distributor (serial data interface at 1200 baud rate, TBS04, TekBox, Saigon, Vietnam)
104 connected to six TDR-sensors (TDR310H, Acclima, Meridian, USA) and attached to an outdoor remote terminal unit (RTU)
105 fully LoRaWAN compliant (TBS12B: 4+1 channel analogue to SDI-12 interface for 24 Bit A/D conversion of sensor signals,
106 TekBox, Saigon, Vietnam) was installed. The Dribox was deployed at least 0.3 m below ground to allow normal field traffic
107 and soil tillage. The sensors and boxes were installed between August and November 2020. At two georeferenced locations,
108 TDR-sensors were installed in 0.3, 0.6 and 0.9 m depth, respectively, approximately 2 m apart from the Driboxes in angles
109 between 45° and 60°. Soil sensors at 0.3 m were placed horizontally, while sensors at 0.6 and 0.9 m depth were placed vertically
110 using auger-made tunnels and extension tubes for soil insertion. Driboxes were autarkic in terms of energy supply, and
111 communication was wireless throughout. Thus no electric cabling except from connections between sensors and Driboxes was
112 needed.

113 The data were recorded every 20 minutes by the LoRa nodes through a LoRa-WAN Gateway DLOS8 (UP GmbH, Ibbenbüren,
114 Germany) which was equipped with the modem TL-WA7510N (TP Link, Hong Kong, China) to transfer the data to a cloud
115 from where collected data could be accessed directly after the measurement. The time series included in this study covered the
116 period from December 01, 2020, until August 14, 2021 (Appendix A). Precipitation and temperature data (Fig. 1) were obtained
117 from two weather stations located in the Eastern and Western end of the main patchCROP field with a 15 min temporal
118 resolution. Climatic water balance was calculated from precipitation and potential evapotranspiration, both measured at the
119 climate station by the German Weather Service in Müncheberg (DWD Climate Data Center (CDC), 2021).

120

121 Furthermore, drone imagery from May 20, 2021, May 31, 2021, and July 06, 2021, was used for vegetation assessment. The
122 drone fixed-wing UAV-based RS eBee platform (SenseFly Ltd., Cheseaux-Lausanne, Switzerland) was operated at noon time
123 and recorded multispectral imagery with a Parrot Sequoia+ camera (green, red, NIR, and red edge bands, spatial resolution of
124 0.105 m) and thermal imagery of the surface (only on May 31, 2021) with a senseFly Duet T camera with a spatial resolution
125 of 0.091 m (Table 2). The multispectral imagery was processed with Pix4D to obtain the Normalized Difference Vegetation
126 Index (NDVI), following Eq. (1):

$$127 \quad NDVI = \frac{NIR-Red}{NIR+Red}$$

128

(1)

129 in which NIR is the intensity of reflected near-infrared light (reflected by vegetation) and Red the intensity of reflected red
130 light (absorbed by vegetation). A digital elevation model with a spatial resolution of 1 m (GeoBasis-DE and LGB, 2021) was
131 used to calculate the slope (ArcGIS 10.7.0; ESRI, 2011) (Table 2).

132

133 Manual soil texture analysis by layer was carried out for part of the sensors by using a Pürckhauer soil auger of 1 m length in
134 eight of twelve analysed patches. Manual soil textural class was estimated at the field by applying the protocol “Finger test to
135 determine soil types according to DIN 19682-2 and KA5” (Sponagel et al., 2005). Additionally, representative soil samples
136 were collected and analysed at the laboratory to determine particle size distribution (based on the German particle
137 classification) by using the traditional gravimetric sieving method. To extrapolate the soil particle distribution from the
138 laboratory to the manual soil textural classes, the high and low yield potential laboratory samples were pooled separately and
139 the average soil particle distribution by soil textural class was calculated and assigned to the respective soil layer with that
140 particular soil textural class. The soil texture analysis showed that soil texture variability increased with depth. In the third
141 layer (average bottom depth = 92 cm), the sand and clay share across 133 sampling points varied between 53% to 94% and
142 2% to 22%, respectively. Soil sample points were between approximately 0.8m and 2.5m far from sensors. The transferability
143 of texture information from the sampling point to the sensor location was not ensured due to high nugget effects. Furthermore,
144 manual soil texture analysis data were not available for all analysed patches. Consequently, they were not included into further
145 correlation analysis.

146 In October 2019, the “Geophilus” soil scanner system (Lueck and Ruehlmann, 2013) was used in the entire field to map
147 electrical resistivity (ERa) of the soil as a proxy for soil texture for the top soil, using reference soil samples to calibrate the
148 readings. The “Geophilus” system is based on sensor fusion of with ERa sensors coupled with a gamma (γ) sensor. Apparent
149 electrical conductivity was measured by pulling one or more sensor pairs mounted on wheels across the field where each pair
150 of sensors measured a different soil depth. Amplitude and phase were measured simultaneously using frequencies from 1 MHz
151 to 1 kHz. Reference soil samples were taken in several points and served as calibration information in order to estimate sand,
152 silt and clay content in the top 0.25 m of soil. A non-linear regression model was applied. The RMSE of sand content (5.7%)
153 was considerably smaller than the standard deviation of the sand content in the first layer from the manual soil texture analysis
154 (11.9%), indicating a satisfactory prediction performance. The γ -sensor was used to minimize uncertainties, being less sensitive
155 to soil moisture than the ERa readings (Bönecke et al., 2021). The estimated sand content in the upper 0.25 m at the study site
156 varied between 69.1% and 81.2% and averaged 79.0% (Table 1, Figure 2).

157 **2.4 Data processing**

158 Soil moisture data were available at 20-minute intervals. Transmission failures due to discharged batteries, signal disturbances
159 in sinks after rainfall, patches with a high density of biomass (e.g. maize), and theft of parts of the monitoring system led to
160 data gaps that amounted to 81 out of 257 days of the measuring period, which were therefore skipped for the analysis. Whereas
161 time series of eight sensors were excluded due to a higher frequency of transmission failures, in total, 64 time series were used

162 for the analysis, and additional data gaps for single sensors were interpolated linearly. Of all 20,668 interpolated gaps, 96%
163 were shorter than two hours, 3% between two and six hours and 1% longer than six hours. In 26 cases, gaps exceeded the
164 duration of one day. The interpolation was justified as the differences between the values before and after the gaps were within
165 the measuring accuracy of 1 vol-% of the TDR sensors (Acclima Inc., 2019). To ensure equal weighting for the subsequent
166 analysis all soil moisture time series were z-transformed to unit variance and zero mean each (cf. Hohenbrink and Lischeid,
167 2015). As a consequence, differences of absolute values were not considered by the further analysis.

168 **2.4 Statistical analysis**

169 To identify common temporal patterns among single time series, the soil moisture data set was analysed by a principal
170 component analysis (PCA). In a first step, PCA decomposes the total variance of a multivariate data set into independent
171 fractions called principal components (PCs). The number of PCs is the same as the number of time series in the input data set.
172 Each PC consists of eigenvectors (loadings), scores, and eigenvalues. The scores reflect the temporal dynamics. The
173 importance of single principal components for single sites is represented by the loadings of each PC (Jolliffe, 2002; Lehr and
174 Lischeid, 2020). Loadings are the Pearson correlation coefficients of the single time series of the input data set with the scores
175 of each PC, respectively. The eigenvalues of the single PC are proportional to the variance that they explain. The PCs are
176 sorted in descending order of eigenvalues. Eigenvalues greater than one indicate that a PC explains more variance than a
177 single input time series could contribute to the total variance of the entire input data set (Kaiser, 1960). More details on principal
178 component analysis for time series analysis are found in Jolliffe (2002). The PCA was performed using the *prcomp* function in
179 R version 4.1.0 (R Development Core Team, 2021).

180 The scores of the principal components constitute time series. Every observed time series can be presented at arbitrary precision
181 as a combination of various principal components. When the data set consists of time series of the same observable measured
182 at different locations, the first principal component describes the mean behaviour inherent in the data set. Subsequent principal
183 components reflect typical modifications of that mean behaviour at single locations due to different effects. Thus generating
184 synthetic time series as linear combinations of the first PC and another additional PC helps to assign this additional PC to a
185 specific effect. To that end, scores of that component have either been added to or subtracted from those of the first component
186 using arbitrarily selected factors. The two resulting graphs show how the respective PC causes deviations from the mean
187 behaviour of the data set.

188 The relations to soil and vegetation parameters were tested by computing the Pearson correlation coefficients between the
189 scores and arithmetic mean values of all input time series as well as the Pearson correlation coefficients between loadings and
190 sand content, sensor depth, antecedent z-transformed water contents, slope, and drone imagery products (NDVI and surface
191 temperature). Eventually, the Wilcoxon-Mann-Whitney test was applied to check whether loadings can be grouped by
192 management parameters (crops, cover crops, weeding management). All statistical analyses were conducted with R version
193 4.1.0 (R Development Core Team, 2021).

194 **3 Results**

195 The principal component analysis yielded five components with Eigenvalues exceeding one, which accounted for >97% of the
196 total variance of the data set (Table 4).

197 **3.1 First principal component**

198 The first principal component explained 72.3% spatiotemporal variance of the data set. All loadings on the first PC were
199 negative (Appendix B). The Pearson correlation coefficient of the scores of the first principal component with the mean values
200 of all input time series was less than - 0.999 ($p < 0.01$), the correlation between the scores and the cumulative climatic water
201 balance ($P - ET_p$) was -0.969 ($p < 0.01$). Thus, the time series of the negative scores of this component represented the mean
202 behaviour of soil moisture driven by external factors such as precipitation, temperature, and seasons in general which affected
203 time series in the same way, although to different degrees (cf., Hohenbrink et al., 2016; Lischeid et al., 2021).

204 **3.2 Second principal component**

205 The second principal component explained 17.0% of the total variance. The loadings ranged from -0.801 to 0.760 with a
206 median of -0.030 (Figure 3). The loadings showed a crop type specific pattern. All winter crops (barley, oats, rye) had positive
207 loadings with only one exception in 0.9 m depth. The summer crops maize, soy, and sunflower exhibited negative loadings. In
208 contrast, the summer crop lupine exhibited mostly positive loadings, similar to the winter crops, although of slightly smaller
209 magnitude. According to the Wilcoxon-Mann test, the group of barley, oats, rye, and lupine differed significantly from the
210 group of maize, soy, and sunflower.

211 As described in the Methods section, synthetic time series were generated as a linear combination of PC1 and PC2 (Figure 4).
212 The graph resulting from applying a positive factor for PC2 represents a typical deviation from mean behaviour for sites that
213 exhibit positive loadings, e.g., winter crops (blue line). The opposite holds for the summer crops which load negatively with
214 PC2 (orange line). Both lines plot very close to each other in February and March. In contrast, the orange line shows lower
215 values than the blue line in December and January, indicating lower soil moisture at the summer crop patches. The inverse
216 holds for the subsequent summer period starting in early June, pointing to earlier and more rapid water uptake of the winter
217 crops. In July and August, the approximately constant level of the blue curve indicates that only summer crops continue to
218 consume water while winter crops are in their ripening phase and eventually harvested.

219 Lupine and sunflower were the summer crops which were sown first (March 30, 2021, and April 2, 2021, respectively). Maize
220 was sown on April 16, 2021, and soy on May 15, 2021. The loadings of lupine, which were rather performing like winter crops
221 than summer crops, indicated that lupine showed an early onset of intensive evapotranspiration, compared to other summer
222 crops, especially sunflower which was sown at the same time.

223 For further investigation of the vegetation effect on PCs, the loadings of PC2 were compared to drone imagery taken at the
224 end of May, when sowing has been completed on all patches, and images taken at the beginning of July during winter crops'

225 ripening phase. The second PC's loadings of the time series from different sensors were compared to the Normalized
226 Difference Vegetation Index (NDVI) and surface temperature (only available for May 31, 2021) of the respective sensor
227 location as a proxy for actual evapotranspiration (Table 3). At the end of May, the NDVI, as a proxy for photosynthesis
228 potential, was positively correlated with the loadings. Surface temperature exhibited a negative correlation. The spatial pattern
229 of surface temperature is assumed to be inversely related to that of actual evapotranspiration. Thus, both proxies, NDVI and
230 surface temperature, support the inference that positive loadings on this principal component represent sites with above-
231 average plant activity and root water uptake at the end of May. This holds for sensors from all depths but was the closest for
232 0.9 m depth (Pearson correlation of $r = -0.916$ for surface temperature and of $r = 0.946$ for NDVI on May 31). The results in
233 July compared to those in May support the observation. At the time when the winter crops are already in the ripening phase
234 and the summer crops reach high levels of evapotranspiration, the correlations are being reversed and negative loadings
235 indicate above-average plant activity for summer crops. On July 06, highest Pearson correlations for NDVI are found for 0.6
236 m depth ($r = -0.917$).

237 **3.3 Third principal component**

238 The third PC explained 4.1% of the total data set's variance. Loadings ranged between -0.787 and 0.244 with a median of
239 0.006. Extreme loadings (<-0.25) were found only for sensors in 0.9 m depth in patches 66, 89, 95 and 102 (Figure 5). The
240 location of the patches roughly follows an east-west direction, which, however, cannot be assigned to topography or structures
241 apparent on the topsoil map (Figure 2). Loadings were closely related to the minima of the z-transformed soil moisture in the
242 period from December to February ($r = 0.70$). The most obvious difference between the orange line (negative loading on PC3)
243 and the blue line (positive loading on PC3) during the first half of the study period is that the latter reaches a maximum of soil
244 moisture after rainfall much earlier compared to the former (Figure 6).

245 **3.4 Fourth principal component**

246 The fourth PC explained 2.2% of the total data set's variance. The loadings were clustered by crop groups. All fallow patches
247 showed consistent positive loadings while the patches which were covered by winter crops, showed mainly negative loadings
248 except in patch 95 where the loadings of the two sensors in 0.3 m depth were slightly above zero (Figure 7). According to the
249 Wilcoxon-Mann test treatment group B (fallow, followed by summer crops) differed significantly from group A (winter crops)
250 and C (cover crops, followed by summer crops) whereas there was no significant difference between group A and C. In contrast
251 to crop groups A and B, patches that were covered by the cover crop phacelia during the winter months, did not show one-
252 directional loadings.

253 Figure 8 illustrates the effect of the fourth PC on time series. A positive factor would be typical for more sandy soils and for
254 patches with fallow in autumn and winter (blue line). In contrast the orange line depicts behaviour in more loamy soils and for
255 winter crops. The latter line exhibits slightly more delayed responses to rainstorms and subsequent less steep recovery as it

256 would be expected for more loamy soils. However, it is not clear how winter crops on the one side and fallow on the other side
257 could induce such a different behaviour.

258 **3.5 Fifth principal component**

259 The fifth PC explained 1.7% of the data set's variance. The loadings showed a depth-related pattern. All time series from the
260 0.3 m depth exhibited negative loadings with two minor exceptions. Whereas all time series from 0.9 m depth showed positive
261 loadings throughout, and time series from 0.6 m depth plot in between. Loadings in 0.6 m depth and 0.9 m depth were mostly
262 more similar to each other than to the loadings of 0.3 m depth (Figure 9). The Pearson correlation coefficient between loadings
263 and depth was $r = 0.710$ ($p < 0.05$). Thus it can be concluded that the fifth PC reflected the effect of soil depth on soil moisture
264 variance. This effect differed between crops, with the three most negative loadings found in maize patches while the three
265 most positive loadings were found in lupine patches.

266 The hydrological signal after rainfall events exhibits damping over depth (blue line) while sensors in the upper layer react with
267 a higher sensitivity (orange line) to weather conditions (Figure 10).

268 Neither patterns in topography nor in weeding management modes were reflected in the loadings of PC1-PC5. Due to the lack
269 of subsurface soil data, no additional findings could be derived from the Geophilus texture analysis.

270 **4 Discussion**

271 The first five principal components described about 97% of the variance of the data set, which consisted of observed time
272 series from 64 soil moisture probes and revealed various effects of weather, soil texture, soil depth, crops and management
273 schemes (Table 1). The first principal component captured 72% of the total variance. Consequently, 72% of the observed
274 dynamics could be described by a lumped model that would not consider any within-field heterogeneity. This figure is in the
275 range of similar studies. In the study of Martini et al. (2017), the first PC explained 58% of the variance of a data set that
276 comprised both agricultural fields as well as grassland transects. Lischeid et al. (2017) ascribed 70% of the variance of a forest
277 soil hydrological data set to a single component. In the study by Hohenbrink et al. (2016), 85% of the variance of soil
278 hydrological data in a set of arable field experiments with two different crop rotation schemes was attributed to the first
279 principal component.

280 **4.1 Crop effects**

281 As Korres et al. (2015) stated, the main causes for spatial variability of soil moisture in agricultural fields besides soil
282 parameters are vegetation and management (e.g. planting and harvesting dates). The quantification of the impact of these
283 effects on soil moisture variability is highly important, for instance for hydrological applications and adopted management
284 practices in agriculture (Hupet and Vanclooster, 2002). Joshi and Mohanty (2010) investigated the spatial soil moisture
285 variability on the field to regional scale in the Southern Great Plains regions in the US by means of PCA and assessed the

286 effect of vegetation as limited since none of the first seven PC showed strong correlations with vegetation parameters. In
287 Western China, Wang et al. (2019) used a non-linear Granger causality framework and quantified the vegetation effect on soil
288 moisture variability with up to 8.2%.

289 In this study, conducted at the field scale, around 17% of the total variance was attributed to the vegetation effect. When not
290 considering the temporal component reflected by PC1 and thus only looking at the spatial variability, 61% of the remaining
291 variance (attributed to PC2 to PC64) is caused by the vegetation effect reflected by PC2. Korres et al. (2010) also used PCA
292 to identify the drivers of spatial variability of soil moisture within a cropped area but did not find such a pronounced vegetation
293 effect. In their study more than two thirds of the spatial variability was related to soil parameters and topography. In contrast,
294 the strong influence of vegetation in our study may be due to the high level of crop diversification. Within single crop fields,
295 vegetation effects are observable due to heterogeneous biomass or root development (Brown et al., 2021; Korres et al., 2010),
296 but may be of a lower magnitude compared to fragmented field arrangements with different crops. The high impact of crop
297 diversification on soil moisture variability is also visible when comparing our results to the results of a field under comparable
298 conditions in the same region with only two crop rotations in which only 3.8% was explained by the different crop rotations
299 (Hohenbrink et al., 2016).

300 It needs to be considered that the proportion of the vegetation effect on soil moisture variability does not only vary spatially
301 and over depth, but also over time. Under dry conditions, soil-plant interactions prevail while under moist conditions,
302 percolation behaviour is predominant (Baroni et al., 2013). The scores are time series and reflect the effect size of a particular
303 process represented by the respective PC. The more the scores of a certain PC deviate from zero during specific periods, the
304 stronger the respective effect is. Consequently, the time series of PC2 scores indicates that the effect of vegetation on total
305 variability varies by time. In accordance with literature, the absolute values of the scores of PC2, representing differences
306 between the contrasting seasonality of crops, are highest in the dry months May to August. In the moist winter months January
307 to March, as well as during the heavy rainfall event in July, the scores of PC2 are relatively small, showing that spatial
308 variability at that time is caused by other factors.

309 The second principal component clearly differentiated between winter and summer crops, which was driven by the different
310 seasonal patterns of root water uptake (Figure 3). In contrast, the fourth component separated winter crops and fallow (Figure
311 7). Note that the term “fallow” refers to crop cover in autumn and winter only. Phacelia is grown as a cover crop and usually
312 dies off in frost periods. However, due to rather mild winter temperature this did only partly happen in the study period. Thus
313 some Phacelia patches exhibited negative loadings, similarly to the winter crop patches. Hence the fourth component obviously
314 reflected the effect of plant cover in the winter period, which can hardly be ascribed to different patterns of root water uptake.
315 According to this component, soil moisture dynamics at the fallow patches resembled more the typical behaviour one would
316 expect for sandy soils, and that of winter crop patches a more damped behaviour typical of more loamy soils. That feature
317 could point to a soil carbon effect on the soil’s water holding capacity: Only at the winter crop sites organic carbon in soil
318 increased continuously due to root growth and root exudation, whereas mineralisation reduced the organic carbon stock at the
319 fallow sites. Effects of dense living root networks on soil hydraulic conductivity have been reported, e.g., Scholl et al. (2014),

320 Zhang et al. (2021) and Lange et al. (2013). Further soil-vegetation interactions might play a role, such as soil organic matter
321 from cover crops and plant residues (Manns et al., 2014; Rossini et al., 2021). Usually, such effects are assumed to occur only
322 at larger time scales, which is closely related to problems of detecting changes soil organic carbon quantity or quality. So far
323 there is only anecdotal evidence for rather short-term soil organic carbon quality affecting soil hydraulic properties even at
324 smaller time scales. Although this effect constituted only a minor share of soil moisture variance (Table 4), it was clearly
325 discernible as a separate principal component. This effect would be worth to be tested in more detailed studies. If it were to be
326 confirmed, it would be a good example for how crop management shapes soil properties.

327 **4.2 Soil texture effects**

328 Texture is another highly important spatial variable that affects soil moisture. The pore size distribution, which is directly
329 linked to texture has great influence on wetting processes as well as on the water retention capacity of soil (Krauss et al., 2010;
330 Rossini et al., 2021). Furthermore, texture influences the evapotranspiration which is another main factor controlling soil
331 moisture (Pan and Peters-Lidard, 2008). For coarse grained soils as they are present in this case study, the water retention
332 capacity is small, resulting in enhanced seepage fluxes (Scheffer and Schachtschabel, 2002; Krauss et al. 2010).

333 Loadings on the third principal component were not related to crop types. In contrast, a spatial pattern emerged: Only sensors
334 from 0.9 m depth from six adjacent patches exhibited strongly negative loadings (Figure 2), whereas all other sensors showed
335 minor positive or negative loadings. This points to an effect of subsoil substrates, that is, higher clay content and consequently
336 higher water holding capacity. That would be consistent with delayed response to seepage fluxes and reduced desiccation in
337 the vegetation period (Figure 6). Data on the texture at the sensor location in deeper layers would be of high value to confirm
338 the assumptions.

339 Whereas the third principal component seems to reflect a local peculiarity, the fifth component obviously grasps a more generic
340 feature. Loadings on this component are clearly related with depth (Figure 9). Strong positive loadings indicate a strongly
341 damped behaviour of soil moisture time series: The blue line, representing sites with positive loadings on PC5 which is typical
342 for sensors at greater depth (Figure 9), exhibits clearly reduced amplitudes compared to the orange line, that is, sensors at
343 shallow depth (Figure 9, Figure 10). Hohenbrink and Lischeid (2015) combined a hydrological model and principal component
344 analysis to study the effect of soil depth and soil texture on damping of the input signal in more detail. A subsequent field
345 study proved the relevance of that effect in a real-world setting (Hohenbrink et al., 2016). Moreover, Thomas et al. (2012)
346 found that damping accounted for a large share of variance in a set of hydrographs from a region of 30,000 km². Damping was
347 also the most relevant driver of spatial variance in a set of time series of groundwater head at about the same scale (Lischeid
348 et al., 2021).

349 **5 Conclusion**

350 To disentangle and to quantify different effects of environmental processes in complex settings is a key challenge of
351 agricultural and environmental research. It is an indispensable prerequisite for tailored field and crop management. Mechanistic
352 models are a way to upscale findings from numerous single cause-single effect studies. But there is urgent need to further
353 validate model results and to study interactions between various effects in a systematic way. Principal component analysis is
354 a step further to meet these challenges although not entirely without problems. In this study which focuses on the interplay
355 between crops and soil heterogeneities in terms of soil moisture dynamics, the strength of the methodology in contributing to
356 disentangling different effects of complex spatially and temporally diversified cropping systems based on a comprehensive
357 real-world data set is presented. More than 97% of the observed spatial and temporal variance was assigned to five different
358 effects. Meteorological drivers explained 72.3% of the total variance. Different seasonal patterns of root water uptake of winter
359 crops compared to summer crops accounted for another 17.0% of variance. An additional share of 2.2% of variance seemed
360 to be related to the effects of a living rooting system on soil hydraulic properties. Heterogeneity of subsoil substrates explained
361 4.1 % of variance, and the damping effect of input signals in the soil another 1.7%. To summarize, plant-related direct and
362 indirect effects accounted for 19.2% of the variance, and soil-related effects only for 5.8%. In particular, the plant-induced
363 effects on soil hydraulic properties would be worthwhile to be studied in more detail.

364 Knowledge from data-driven approaches can support adequate crop selection as a management option to encounter the
365 increasing drought risk in the study region. It has been shown that principal component analysis has a high value for the
366 application in environmental sciences, as it allows to draw conclusions about variabilities in large data sets from real-world
367 monitoring setups despite gaps in time series. Information from this study will contribute to elucidate management effects as
368 well as to develop both parsimonious and tailored mechanistic models. Findings of this study highly depend on local
369 conditions. However, we consider the presented approach generally applicable to a large range of site conditions. In this regard,
370 principal component analysis of soil moisture time series performed as a powerful diagnostic tool and is highly recommended.

371 **Acknowledgments**

372 The maintenance of the patchCROP experimental infrastructure and the LoRaWAN soil sensor system is ensured by the
373 Leibniz Centre for Agricultural Landscape Research. The authors acknowledge the additional support from the German
374 Research Foundation under Germany's Excellence Strategy, EXC-2070 – 390732324 – PhenoRob for patchCROP related
375 research activities.

376 The authors thank Gerhard Kast, Thomas von Oepen, Lars Richter, Robert Zieciak, Sigrid Ehlert and Motaz Abdelaziz for
377 their dedicated support in maintenance of the monitoring system and data collection.

378 **Competing interests**

379 The authors declare that they have no conflict of interest.

380 **References**

381 Acclima Inc.: True TDR310H. Soil-Water-Temperature-BEC-Sensor, 2019.

382 Alhameid, A., Singh, J., Sekaran, U., Ozlu, E., Kumar, S., and Singh, S.: Crop rotational diversity impacts soil physical and
383 hydrological properties under long-term no- and conventional-till soils, *Soil Res.*, 58, 84, <https://doi.org/10.1071/SR18192>,
384 2020.

385 Baroni, G., Ortuani, B., Facchi, A., and Gandolfi, C.: The role of vegetation and soil properties on the spatio-temporal
386 variability of the surface soil moisture in a maize-cropped field, *Journal of Hydrology*, 489, 148–159,
387 <https://doi.org/10.1016/j.jhydrol.2013.03.007>, 2013.

388 Birthal, P. S. and Hazrana, J.: Crop diversification and resilience of agriculture to climatic shocks: Evidence from India,
389 *Agricultural Systems*, 173, 345–354, <https://doi.org/10.1016/j.agsy.2019.03.005>, 2019.

390 Bogena, H. R., Weuthen, A., and Huisman, J. H.: Recent Developments in Wireless Soil Moisture Sensing to Support Scientific
391 Research and Agricultural Management, *Sensors*, 22, 9792, <https://doi.org/10.3390/s22249792>, 2022.

392 Bönecke, E., Meyer, S., Vogel, S., Schröter, I., Gebbers, R., Kling, C., Kramer, E., Lück, K., Nagel, A., Philipp, G., Gerlach,
393 F., Palme, S., Scheibe, D., Zieger, K., Rühlmann, J.: Guidelines for precise lime management based on high-resolution soil
394 pH, texture and SOM maps generated from proximal soil sensing data, *Precision Agric*, 22, 493-523,
395 <https://doi.org/10.1007/s11119-020-09766-8>, 2021.

396 Bretherton, C. S., Smith, C., and Wallace, J. M.: An intercomparison of methods for finding coupled patterns in climate data,
397 *Journal of Climatology*, 5, 541–560, 1992.

398 Brocca, L., Melone, F., Moramarco, T., and Morbidelli, R.: Spatial-temporal variability of soil moisture and its estimation
399 across scales, *Water Resour. Res.*, 46, <https://doi.org/10.1029/2009WR008016>, 2010.

400 Brown, M., Heinse, R., Johnson-Maynard, J., and Huggins, D.: Time-lapse mapping of crop and tillage interactions with soil
401 water using electromagnetic induction, *Vadose zone j.*, 20, <https://doi.org/10.1002/vzj2.20097>, 2021.

402 Cardell-Oliver, R., Hübner, C., Leopold, M., and Beringer, J.: Dataset: LoRa Underground Farm Sensor Network, in:
403 *Proceedings of the 2nd Workshop on Data Acquisition To Analysis - DATA'19*, the 2nd Workshop, New York, NY, USA,
404 26–28, <https://doi.org/10.1145/3359427.3361912>, 2019.

405 Deumlich, D., Ellerbrock, R. H., and Frielinghaus, Mo.: Estimating carbon stocks in young moraine soils affected by erosion,
406 *CATENA*, 162, 51–60, <https://doi.org/10.1016/j.catena.2017.11.016>, 2018.

407 Donat, M., Geistert, J., Grahmann, K., Bloch, R., and Bellingrath-Kimura, S. D.: Patch cropping- a new methodological
408 approach to determine new field arrangements that increase the multifunctionality of agricultural landscapes, *Computers and*
409 *Electronics in Agriculture*, 197, 106894, <https://doi.org/10.1016/j.compag.2022.106894>, 2022.

410 DWD Climate Data Center (CDC): Historische tägliche Stationsbeobachtungen (Temperatur, Druck, Niederschlag,
411 Sonnenscheindauer, etc.) für Deutschland, Version v21.3, 2021.

412 Fischer, C., Roscher, C., Jensen, B., Eisenhauer, N., Baade, J., Attinger, S., Scheu, S., Weisser, W. W., Schumacher, J.,
413 Hildebrandt, A.: How Do Earthworms, Soil Texture and Plant Composition Affect Infiltration along an Experimental Plant
414 Diversity Gradient in Grassland?, PLoS ONE, 9, 6, <https://doi.org/10.1371/journal.pone.0098987>, 2014.

415 Fischer, G. F., Nachtergaele, S., Prieler, S., van Velthuisen, H. T., Verelst, L., and Wisberg, D.: Global Agro-ecological Zones
416 Assessment for Agriculture (GAEZ 2008), IIASA, Laxenburg, Austria and FAO, Rome, 2008.

417 GeoBasis-DE and Landesvermessung und Geobasisinformation Brandenburg (LGB): Digitales Geländemodell (DGM),
418 Landesvermessung und Geobasisinformation Brandenburg (LGB), Potsdam, 2021.

419 Grahmann, K., Reckling, M., Hernandez-Ochoa, I., and Ewert, F.: An agricultural diversification trial by patchy field
420 arrangements at the landscape level: The landscape living lab “patchCROP,” in: Aspects of Applied Biology, Intercropping
421 for sustainability: Research developments and their application, 385–391, 2021.

422 Hohenbrink, T. L. and Lischeid, G.: Does textural heterogeneity matter? Quantifying transformation of hydrological signals
423 in soils, Journal of Hydrology, 523, 725–738, <https://doi.org/10.1016/j.jhydrol.2015.02.009>, 2015.

424 Hohenbrink, T. L., Lischeid, G., Schindler, U., and Hufnagel, J.: Disentangling the Effects of Land Management and Soil
425 Heterogeneity on Soil Moisture Dynamics, Vadose Zone Journal, 15, <https://doi.org/10.2136/vzj2015.07.0107>, 2016.

426 Hong, Z., Kalbarczyk, Z., Iyer, R. K.: A Data-Driven Approach to Soil Moisture Collection and Prediction, 2016 IEEE
427 International Conference on Smart Computing (SMARTCOMP), St. Louis, MO, USA, 1-6,
428 <https://doi.org/10.1109/SMARTCOMP.2016.7501673>, 2016.

429 Hupet, F. and Vanclooster, M.: Intraseasonal dynamics of soil moisture variability within a small agricultural maize cropped
430 field, Journal of Hydrology, 261, 86–101, 2002.

431 Jolliffe, I. T.: Principal component analysis. Springer Series in Statistics, Springer, New York, 2002.

432 Joshi, C. and Mohanty, B. P.: Physical controls of near-surface soil moisture across varying spatial scales in an agricultural
433 landscape during SMEX02: Physical controls of soil moisture, Water Resour. Res., 46,
434 <https://doi.org/10.1029/2010WR009152>, 2010.

435 Kaiser, H. F.: The Application of Electronic Computers to Factor Analysis, Educ.Psychol. Measur., 20,
436 <https://doi.org/10.1177/001316446002000116>, 1960.

437 Karlen, D. L., Hurley, E. G., Andrews, S. S., Cambardella, C. A., Meek, D. W., Duffy, M. D., and Mallarino, A. P.: Crop
438 Rotation Effects on Soil Quality at Three Northern Corn/Soybean Belt Locations, Agron.j., 98, 484–495,
439 <https://doi.org/10.2134/agronj2005.0098>, 2006.

440 Khan, H., Farooque, A. A., Acharya, B., Abbas, F., Esau, T. J., and Zaman, Q. U.: Delineation of Management Zones for Site-
441 Specific Information about Soil Fertility Characteristics through Proximal Sensing of Potato Fields, Agronomy, 10, 1854,
442 <https://doi.org/10.3390/agronomy10121854>, 2020.

443 Korres, W., Koyama, C. N., Fiener, P., and Schneider, K.: Analysis of surface soil moisture patterns in agricultural landscapes
444 using Empirical Orthogonal Functions, Hydrol. Earth Syst. Sci., 14, 751–764, <https://doi.org/10.5194/hess-14-751-2010>, 2010.

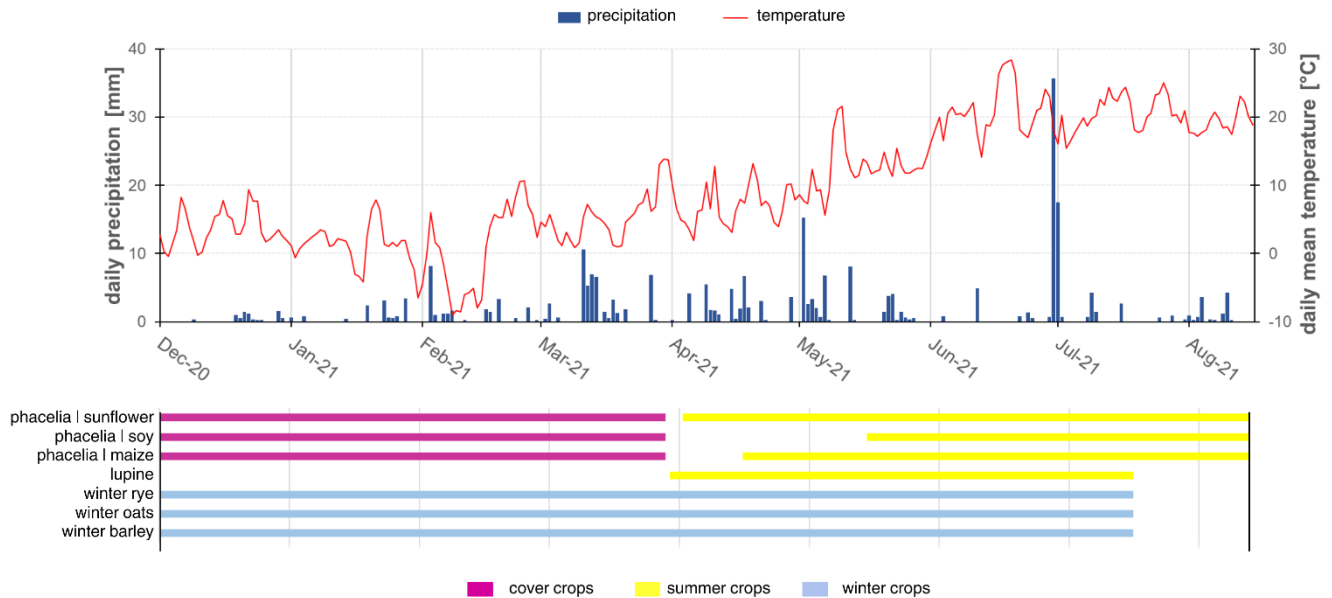
445 Korres, W., Reichenau, T. G., Fiener, P., Koyama, C. N., Bogena, H. R., Cornelissen, T., Baatz, R., Herbst, M., Diekkrüger,
446 B., Vereecken, H., and Schneider, K.: Spatio-temporal soil moisture patterns – A meta-analysis using plot to catchment scale
447 data, Journal of Hydrology, 520, 326–341, <https://doi.org/10.1016/j.jhydrol.2014.11.042>, 2015.

- 448 Koudahe, K., Allen, S. C., Djaman, K.: Critical review of the impact of cover crops on soil properties, *International Soil and*
449 *Water Conservation Research*, 10, 343-354, <https://doi.org/10.1016/j.iswcr.2022.03.003>, 2022.
- 450 Krauss, L., Hauck, C., and Kottmeier, C.: Spatio-temporal soil moisture variability in Southwest Germany observed with a
451 new monitoring network within the COPS domain, *metz*, 19, 523–537, <https://doi.org/10.1127/0941-2948/2010/0486>, 2010.
- 452 Lange, B., Germann, P. F., and Lüscher, P.: Greater abundance of *Fagus sylvatica* in coniferous flood protection forests due
453 to climate change: impact of modified root densities on infiltration, *Eur J Forest Res*, 132, 151–163,
454 <https://doi.org/10.1007/s10342-012-0664-z>, 2013.
- 455 Lehr, C. and Lischeid, G.: Efficient screening of groundwater head monitoring data for anthropogenic effects and measurement
456 errors, *Hydrol. Earth Syst. Sci.*, 24, 501–513, <https://doi.org/10.5194/hess-24-501-2020>, 2020.
- 457 Lischeid, G., Frei, S., Huwe, B., Bogner, C., Lüers, J., Babel, W., and Foken, T.: Catchment Evapotranspiration and Runoff,
458 in: *Energy and Matter Fluxes of a Spruce Forest Ecosystem*, vol. 229, Springer, Cham, Cham, 355–375, 2017.
- 459 Lischeid, G., Dannowski, R., Kaiser, K., Nützmann, G., Steidl, J., and Stüve, P.: Inconsistent hydrological trends do not
460 necessarily imply spatially heterogeneous drivers, *Journal of Hydrology*, 596, 126096,
461 <https://doi.org/10.1016/j.jhydrol.2021.126096>, 2021.
- 462 Lloret, J., Sendra, S., Garcia, L., and Jimenez, J. M.: A Wireless Sensor Network Deployment for Soil Moisture Monitoring
463 in Precision Agriculture, *Sensors*, 21, 7243, <https://doi.org/10.3390/s21217243>, 2021.
- 464 Lueck, E. and Ruehlmann, J.: Resistivity mapping with Geophilus Electricus - Information about lateral and vertical soil
465 heterogeneity, *Geoderma*, 199, 2–11, <https://doi.org/10.1016/j.geoderma.2012.11.009>, 2013.
- 466 Mahmood, R., Littell, A., Hubbard, K. G., and You, J.: Observed data-based assessment of relationships among soil moisture
467 at various depths, precipitation, and temperature, *Applied Geography*, 34, 255–264,
468 <https://doi.org/10.1016/j.apgeog.2011.11.009>, 2012.
- 469 Martini, E., Wollschläger, U., Musolff, A., Werban, U., and Zacharias, S.: Principal Component Analysis of the Spatiotemporal
470 Pattern of Soil Moisture and Apparent Electrical Conductivity, *Vadose Zone Journal*, 16, vzj2016.12.0129,
471 <https://doi.org/10.2136/vzj2016.12.0129>, 2017.
- 472 Nied, M., Hundecha, Y., and Merz, B.: Flood-initiating catchment conditions: a spatio-temporal analysis of large-scale soil
473 moisture patterns in the Elbe River basin, *Hydrol. Earth Syst. Sci.*, 17, 1401–1414, <https://doi.org/10.5194/hess-17-1401-2013>,
474 2013.
- 475 Nunes, M. R., van Es, H. M., Schindelbeck, R., Ristow, A. J., Ryan, M.: No-till and cropping system diversification improve
476 soil health and crop yield, *Geoderma*, 328, 30–43, <https://doi.org/10.1016/j.geoderma.2018.04.031>, 2018.
- 477 Pan, F. and Peters-Lidard, C. D.: On the Relationship Between Mean and Variance of Soil Moisture Fields, *JAWRA Journal*
478 *of the American Water Resources Association*, 44, 235–242, <https://doi.org/10.1111/j.1752-1688.2007.00150.x>, 2008.
- 479 Paroda, Raj. S., Suleimenov, M., Yusupov, H., Kireyev, A., Medeubayev, R., Martynova, L., and Yusupov, K.: Crop
480 Diversification for Dryland Agriculture in Central Asia, in: *CSSA Special Publications*, edited by: Rao, S. C. and Ryan, J.,
481 *Crop Science Society of America and American Society of Agronomy*, Madison, WI, USA, 139–150,
482 <https://doi.org/10.2135/cssaspepub32.c9>, 2015.
- 483 Placidi, P., Morbidelli, R., Fortunati, D., Papini, N., Gobbi, F., and Scorzoni, A.: Monitoring Soil and Ambient Parameters in
484 the IoT Precision Agriculture Scenario: An Original Modeling Approach Dedicated to Low-Cost Soil Water Content Sensors,
485 *Sensors*, 21, 5110, <https://doi.org/10.3390/s21155110>, 2021.

- 486 Prakosa, S. W., Faisal, M., Adhitya, Y., Leu, J.-S., Köppen, M., and Avian, C.: Design and Implementation of LoRa Based
487 IoT Scheme for Indonesian Rural Area, *Electronics*, 10, 77, <https://doi.org/10.3390/electronics10010077>, 2021.
- 488 R Development Core Team: R: A Language and Environment for Statistical Computing, R Foundation for Statistical
489 Computing (Version 4.1.0, <http://www.R-project.org>), Vienna, 2021.
- 490 Rodriguez, C., Mårtensson, L.-M. D., Jensen, E. S., and Carlsson, G.: Combining crop diversification practices can benefit
491 cereal production in temperate climates, *Agron. Sustain. Dev.*, 41, 48, <https://doi.org/10.1007/s13593-021-00703-1>, 2021.
- 492 Rossini, P. R., Ciampitti, I. A., Hefley, T., and Patrignani, A.: A soil moisture-based framework for guiding the number and
493 location of soil moisture sensors in agricultural fields, *Vadose zone j.*, 20, <https://doi.org/10.1002/vzj2.20159>, 2021.
- 494 Salam, A.: *Internet of Things for Sustainable Community Development: Wireless Communications, Sensing, and Systems*,
495 Springer International Publishing, Cham, Switzerland, <https://doi.org/10.1007/978-3-030-35291-2>, 2020.
- 496 Salam, A. and Raza, U.: *Signals in the Soil: Developments in Internet of Underground Things*, Springer International
497 Publishing, Cham, Switzerland, <https://doi.org/10.1007/978-3-030-50861-6>, 2020.
- 498 Scheffer, F. and Schachtschabel, P.: *Lehrbuch der Bodenkunde*, 15th ed., Spektrum Akademischer Verlag GmbH. Berlin,
499 Heidelberg, <https://doi.org/10.1007/978-3-662-55871-3>, 2002.
- 500 Scholl, P., Leitner, D., Kammerer, G., Loiskandl, W., Kaul, H.-P., and Bodner, G.: Root induced changes of effective 1D
501 hydraulic properties in a soil column, *Plant Soil*, 381, 193–213, <https://doi.org/10.1007/s11104-014-2121-x>, 2014.
- 502 Si, B. C.: Spatial Scaling Analyses of Soil Physical Properties: A Review of Spectral and Wavelet Methods, *Vadose Zone*
503 *Journal*, 7, 547–562, <https://doi.org/10.2136/vzj2007.0040>, 2008.
- 504 Sponagel, H., Grottenthaler, W., Hartmann, K.J., Hartwich, R., Janetzko, P., Joisten, H., Kühn, D., Sabel, K.J., Traidl, R.
505 (Eds.): *Bodenkundliche Kartieranleitung (German Manual of Soil Mapping, KA5)*, 5th edition, Bundesanstalt für
506 Geowissenschaften und Rohstoffe, Hannover, 2005.
- 507 Strebelle, S., Payrazyan, K., and Caers, J.: Modeling of a Deepwater Turbidite Reservoir Conditional to Seismic Data Using
508 Principal Component Analysis and Multiple-Point Geostatistics, *SPE Journal*, 8, 227–235, <https://doi.org/10.2118/85962-PA>,
509 2003.
- 510 Tamburini, G., Bommarco, R., Wanger, T. C., Kremen, C., van der Heijden, M. G. A., Liebman, M., and Hallin, S.:
511 Agricultural diversification promotes multiple ecosystem services without compromising yield, *Sci. Adv.*, 6, eaba1715,
512 <https://doi.org/10.1126/sciadv.aba1715>, 2020.
- 513 Taylor, J. and Whelan, B.: *A General Introduction to Precision Agriculture*, 2010.
- 514 Thomas, B., Lischeid, G., Steidl, J., and Dannowski, R.: Regional catchment classification with respect to low flow risk in a
515 Pleistocene landscape, *Journal of Hydrology*, 475, 392–402, <https://doi.org/10.1016/j.jhydrol.2012.10.020>, 2012.
- 516 Trnka, M., Rötter, R. P., Ruiz-Ramos, M., Kersebaum, K. C., Olesen, J. E., Žalud, Z., and Semenov, M. A.: Adverse weather
517 conditions for European wheat production will become more frequent with climate change, *Nature Clim Change*, 4, 637–643,
518 <https://doi.org/10.1038/nclimate2242>, 2014.
- 519 Vachaud, G., Passerat De Silans, A., Balabanis, P., Vauclin, M.: Temporal Stability of Spatially Measured Soil Water
520 Probability Density Function, *Soil Science Society of America Journal*, 49, 822-828,
521 <https://doi.org/10.2136/sssaj1985.03615995004900040006x>, 1985.

- 522 Vanderlinden, K., Vereecken, H., Hardelauf, H., Herbst, M., Martínez, G., Cosh, M. H., Pachepsky, Y. A.: Temporal Stability
 523 of Soil Water Contents: A Review of Data and Analyses, *Vadose Zone Journal*, <https://doi.org/10.2136/vzj2011.0178>, 2012.
- 524 Vereecken, H., Huisman, J. A., Pachepsky, Y., Montzka, C., van der Kruk, J., Bogen, H., Weihermüller, L., Herbst, M.,
 525 Martínez, G., and Vanderborght, J.: On the spatio-temporal dynamics of soil moisture at the field scale, *Journal of Hydrology*,
 526 516, 76–96, <https://doi.org/10.1016/j.jhydrol.2013.11.061>, 2014.
- 527 Wang, Y., Yang, J., Chen, Y., Fang, G., Duan, W., Li, Y., and De Maeyer, P.: Quantifying the Effects of Climate and
 528 Vegetation on Soil Moisture in an Arid Area, China, *Water*, 11, 767, <https://doi.org/10.3390/w11040767>, 2019.
- 529 Yang, L., Chen, L., and Wei, W.: Effects of vegetation restoration on the spatial distribution of soil moisture at the hillslope
 530 scale in semi-arid regions, *CATENA*, 124, 138–146, <https://doi.org/10.1016/j.catena.2014.09.014>, 2015.
- 531 Zhang, J., Li, Y., Yang, T., Liu, D., Liu, X., and Jiang, N.: Spatiotemporal variation of moisture in rooted-soil, *CATENA*, 200,
 532 105144, <https://doi.org/10.1016/j.catena.2021.105144>, 2021.
- 533 Zhao, Y., Peth, S., Wang, X. Y., Lin, H., and Horn, R.: Controls of surface soil moisture spatial patterns and their temporal
 534 stability in a semi-arid steppe, *Hydrol. Process.*, 24, 2507–2519, <https://doi.org/10.1002/hyp.7665>, 2010.

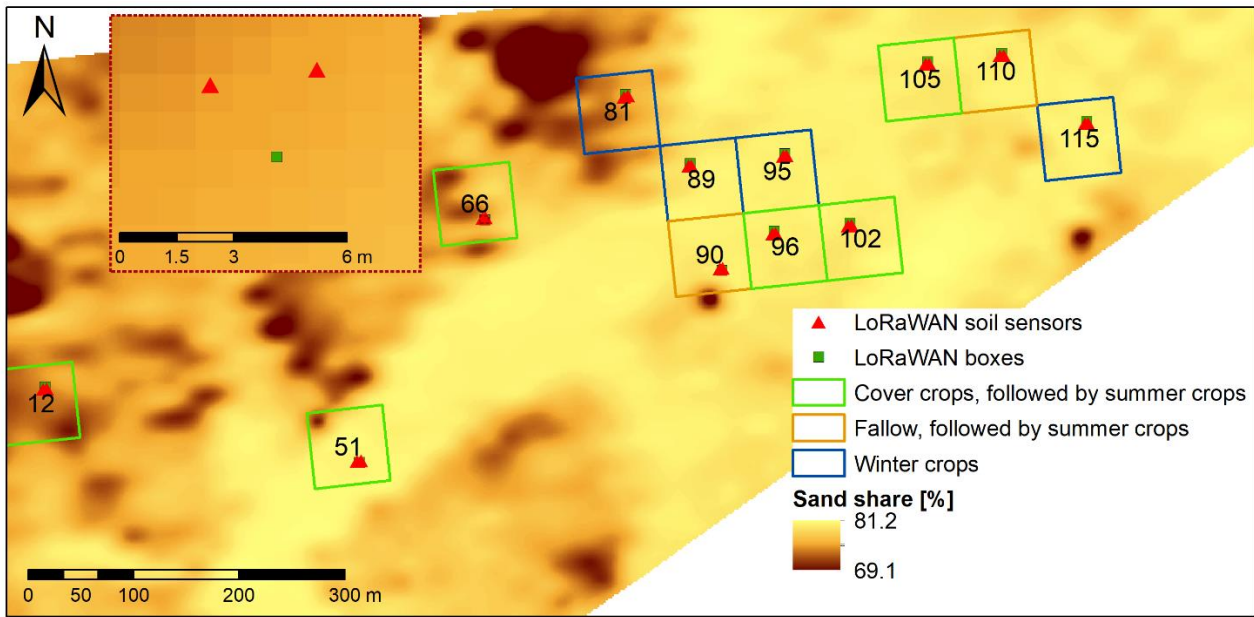
535 **Figures and Tables**



536

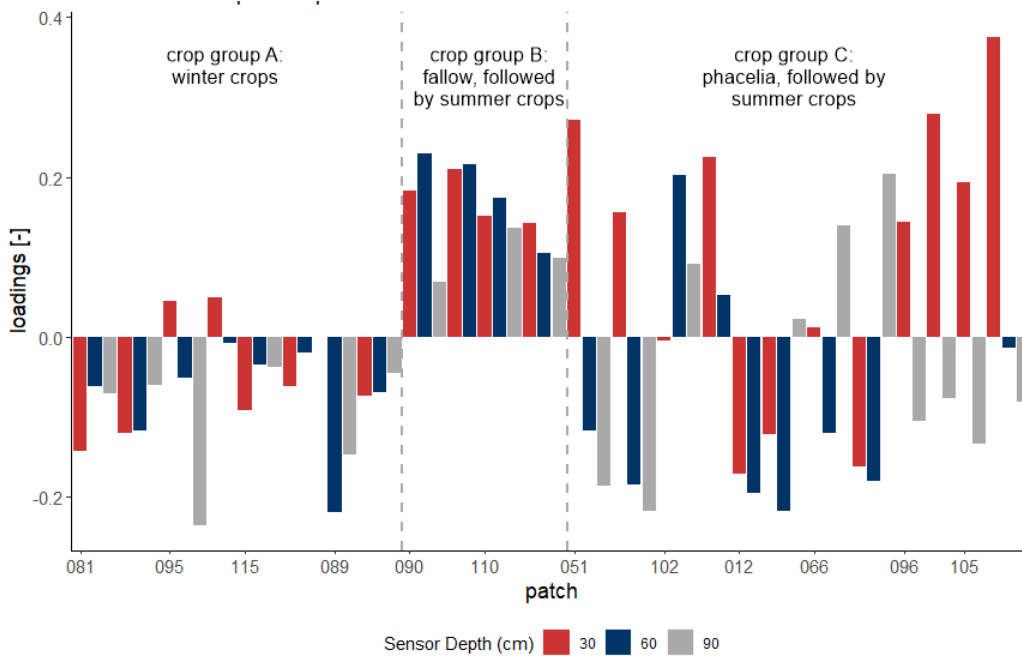
537 **Figure 1: Measured daily precipitation and mean temperature and crops grown from 2020-12-01 until 2021-08-15 at the**
 538 **experimental site in Tempelberg, Brandenburg, Germany.**

539



540

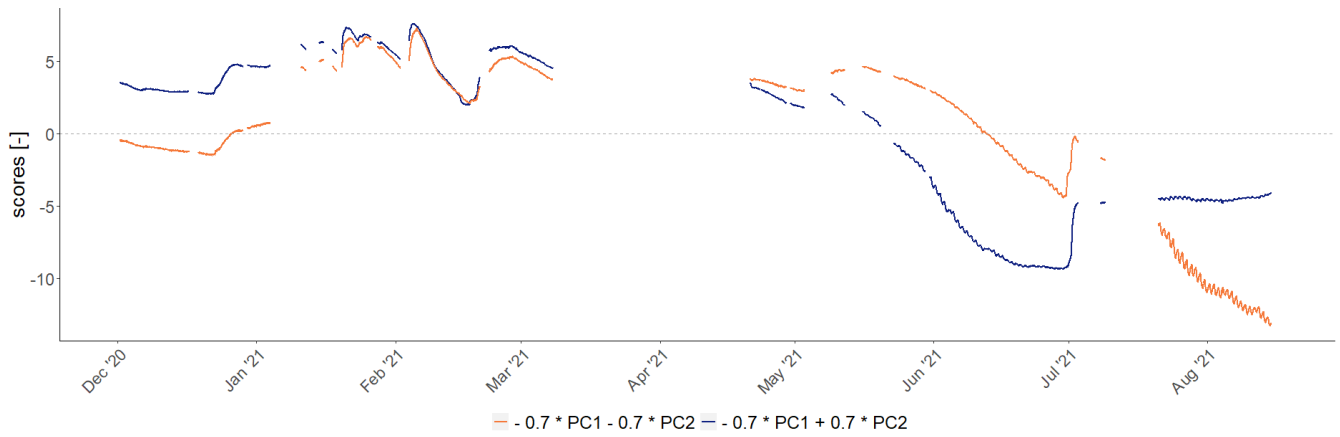
541 **Figure 2: Sand content in the top 0.25 m soil depth and location of the analysed patches including soil sensors under different crop**
 542 **rotations in the landscape laboratory patchCROP, Tempelberg, Brandenburg, Germany. The inset shows sensor and box location**
 543 **within one of the patches.**



544

545 **Figure 3: Loadings of time series on the second principal component. Bars represent individual time series grouped by patch ID**
 546 **and sorted by crop.**

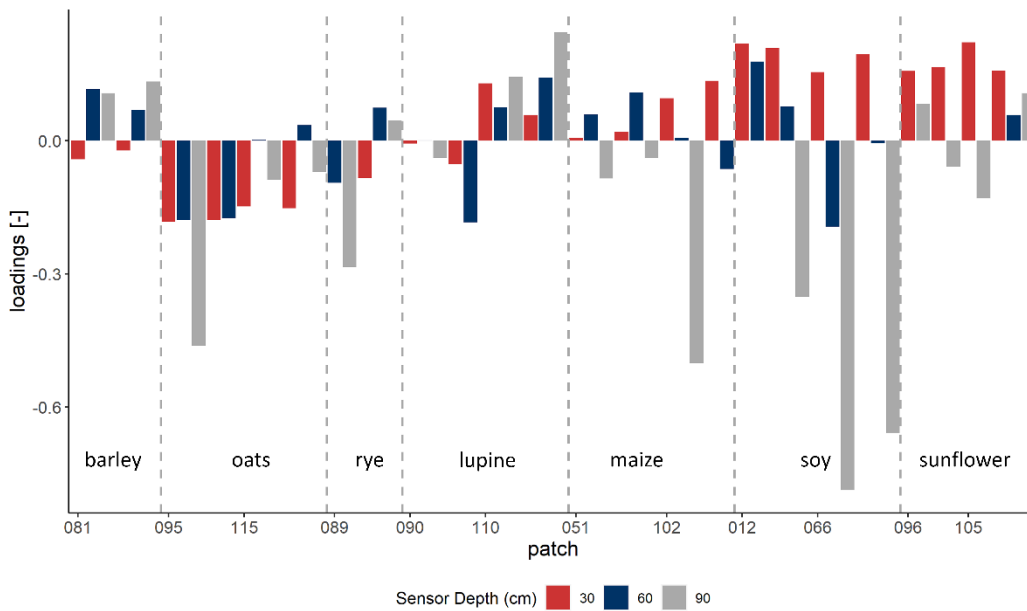
547



548

549 **Figure 4: Effect of the second principal component on modification of the general mean behaviour which is presented by the first**
550 **principal component.**

551



552

553 **Figure 5: Loadings of time series on the third principal component. Bars represent individual time series grouped by patch ID,**
554 **sorted by crop.**

555

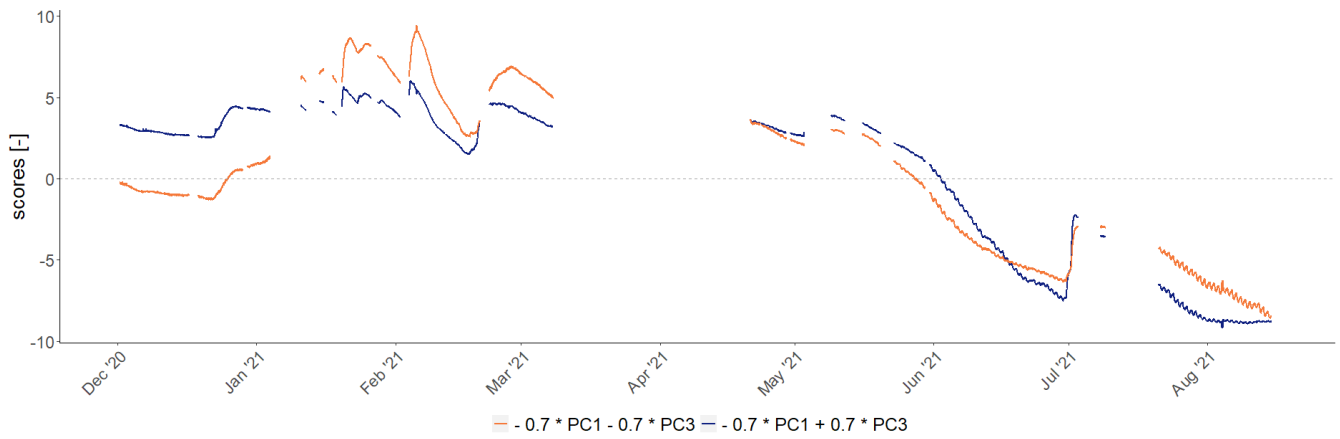


Figure 6: Effect of the third principal component on modification of the general mean behaviour which is presented by the first principal component.

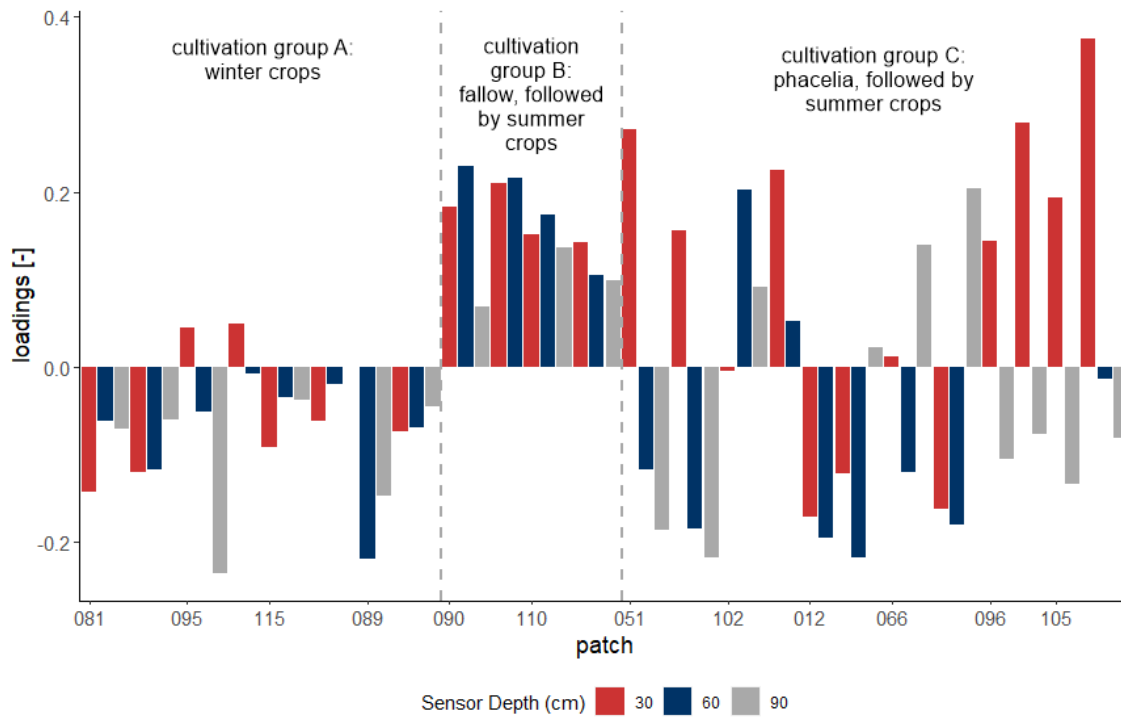
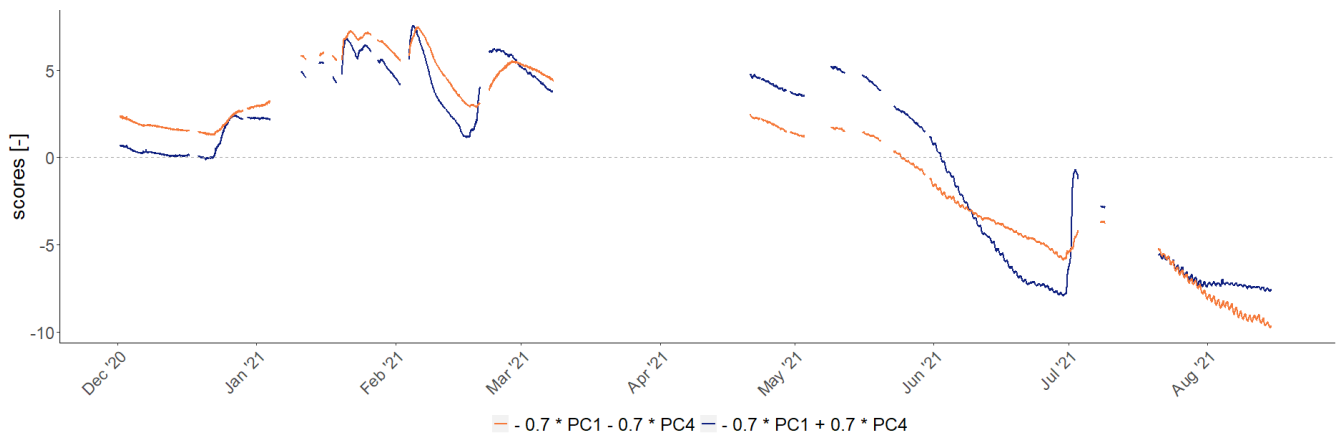


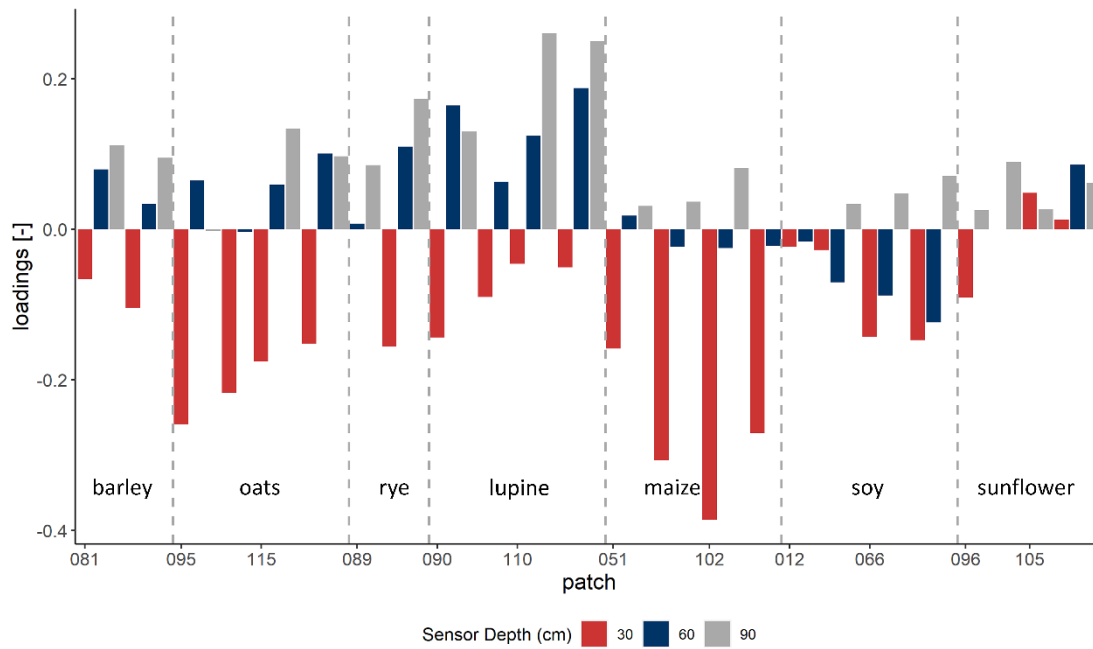
Figure 7: Loadings of time series on the fourth principal component. Bars represent individual time series grouped by patch ID, sorted by treatment group.



562

563 **Figure 8: Effect of the fourth principal component on modification of the general mean behaviour which is presented by the first**
 564 **principal component.**

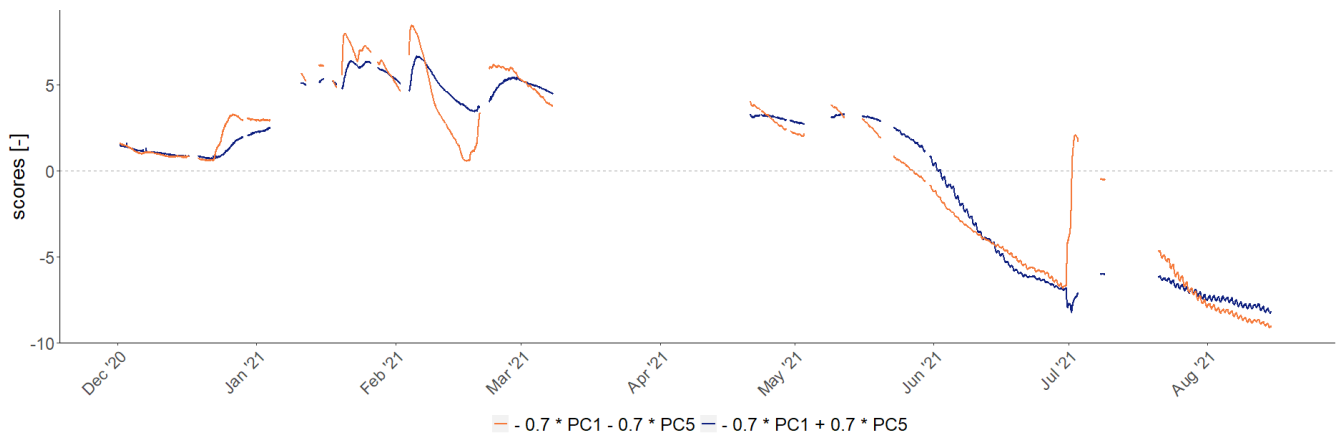
565



566

567 **Figure 9: Loadings of time series on the fifth principal component. Bars represent individual time series grouped by patch ID,**
 568 **sorted by crop.**

569



570

571 **Figure 10: Effect of the fifth principal component on modification of the general mean behaviour which is presented by the first**
 572 **principal component.**

573 **Table 1: Overview of crop rotation, sand content in the top 0.25 m soil depth and weed control of analysed patches.**

Patch ID	Crop in winter season	Crop in summer season	Crop group	Sand content (in 1 m buffer zone around sensors) [%]	Weed control
95	Winter oats		A	80.7	conventional
115	Winter oats		A	80.6	reduced
89	Winter rye		A	80.5	conventional
90	Fallow	Lupine	B	80.6	conventional
110	Fallow	Lupine	B	80.3	reduced
51	Phacelia	Maize	C	80.8	reduced
102	Phacelia	Maize	C	80.6	conventional
12	Phacelia	Soy	C	78.5	reduced
66	Phacelia	Soy	C	77.9	conventional
96	Phacelia	Sunflower	C	80.6	conventional
105	Phacelia	Sunflower	C	80.5	reduced

574

575 **Table 2: Overview of NDVI, surface temperature, and slope at the locations of analysed sensors.**

Crop	Patch ID	Sensor Position	NDVI 2021-05-20 [-]	NDVI 2021-05-31 [-]	NDVI 2021-07-06 [-]	Surface Temperature [°C]	Slope [°]
Barley	81	West	0.874	0.182	0.926	20.57	2.01

Barley	81	East	0.875	0.180	0.927	20.43	1.94
Oats	95	East	0.838	0.208	0.834	27.25	1.36
Oats	95	West	0.838	0.213	0.840	27.85	1.15
Oats	115	West	0.756	0.278	0.845	23.70	1.28
Oats	115	East	0.783	0.281	0.863	25.12	0.43
Rye	89	West	0.796	0.263	0.856	22.39	1.74
Rye	89	East	0.787	0.206	0.822	24.95	1.67
Lupine	90	West	0.185	0.395	0.710	26.31	1.40
Lupine	90	East	0.203	0.391	0.733	24.96	1.27
Lupine	110	West	0.090	0.563	0.635	26.98	1.88
Lupine	110	East	0.090	0.567	0.639	26.76	2.50
Maize	51	West	-0.099	0.654	0.181	35.44	0.82
Maize	51	East	-0.096	0.638	0.217	35.29	0.93
Maize	102	West	-0.077	0.714	0.175	37.88	0.88
Maize	102	East	-0.058	0.728	0.178	38.03	0.90
Soy	12	West	-0.107	0.748	0.166	34.87	1.71
Soy	12	East	-0.108	0.723	0.162	34.44	1.11
Soy	66	West	-0.115	0.730	0.144	35.09	2.40
Soy	66	East	-0.114	0.661	0.147	34.39	2.13
Sunflower	96	West	-0.109	0.816	0.211	33.76	0.59
Sunflower	96	East	-0.101	0.827	0.229	34.70	0.69
Sunflower	105	West	0.178	0.610	0.564	29.79	1.04
Sunflower	105	East	0.030	0.696	0.399	34.53	1.00

576

577 **Table 3: Pearson correlation coefficients between drone imagery products taken on May 31st, 2021, and loadings of sensors in all**
578 **depths or at single depths, respectively, on the second principal component. All correlations are highly significant (p <0.01).**

	Sensors in all depths	0.3 m	0.6 m	0.9 m
Surface temperature	-0.853	-0.881	-0.909	-0.916
NDVI 2021-05-20	0.836	0.904	0.837	0.907
NDVI 2021-05-31	0.899	0.945	0.944	0.946
NDVI 2021-07-06	-0.860	-0.898	-0.917	-0.913

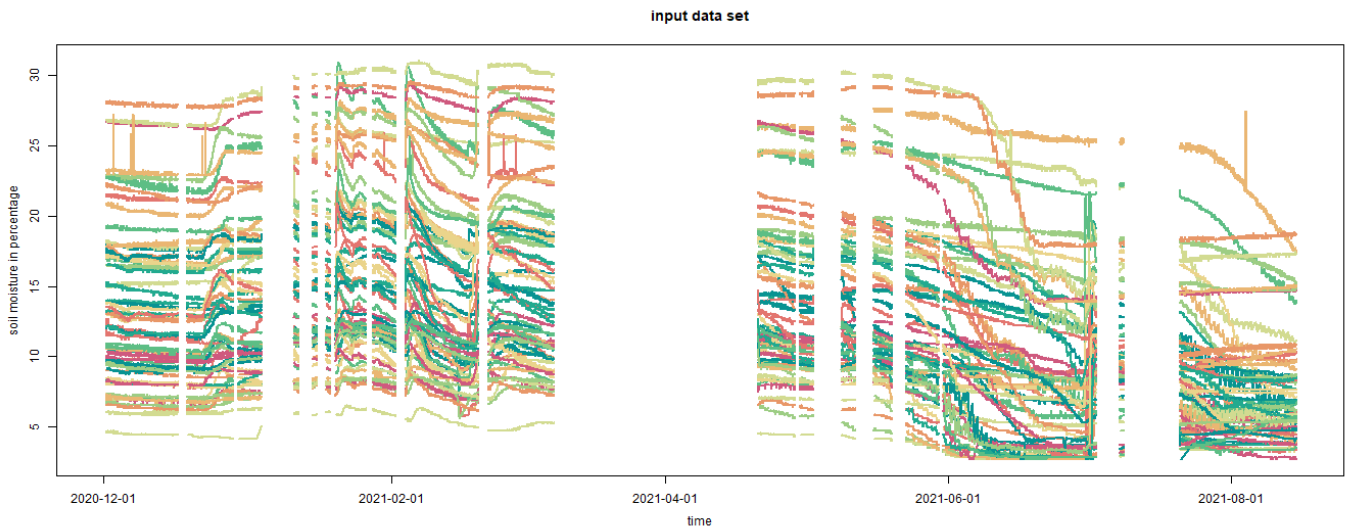
579

580 **Table 4: Principal components 1 to 5.**

	PC1	PC2	PC3	PC4	PC5
Eigenvalue	46.25	10.89	2.60	1.43	1.06
Proportion of variance [%]	72.27	17.01	4.06	2.23	1.65
Proportion of variance (cumulative) [%]	72.27	89.28	93.34	95.57	97.22
Interpretation	Mean behaviour	Winter vs. summer crops	Subsoil texture	Soil organic carbon	Damping of the input signal
Prevailing driver	weather	crop	soil	crop and soil	soil

581

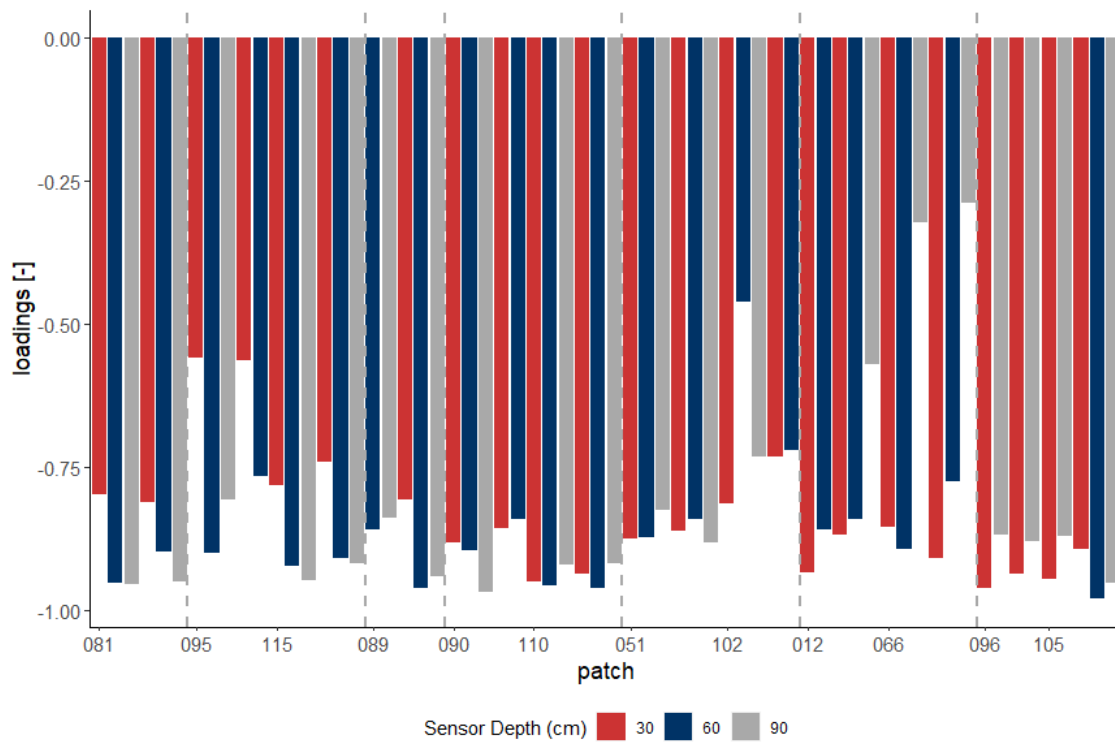
582 APPENDIX A



583
584 **Figure 11: Soil moisture data from 64 sensors in different depths as input data set.**

585 APPENDIX B

586



587

588 **Figure 12: Loadings of time series on the first principal component. Bars represent individual time series grouped by patch ID,**
 589 **sorted by crop.**

590